



## Discrete element method for effective thermal conductivity of packed pebbles accounting for the Smoluchowski effect

M. Moscardini<sup>a,\*</sup>, Y. Gan<sup>b</sup>, S. Papeschi<sup>a</sup>, M. Kamlah<sup>a</sup>

<sup>a</sup> Institute for Applied Materials, Karlsruhe Institute of Technology (KIT), Germany

<sup>b</sup> School of Civil Engineering, The University of Sydney, Sydney, NSW, 2006, Australia



### ARTICLE INFO

#### Keywords:

Effective thermal conductivity  
Smoluchowski effect  
Pebble beds  
Breeder blanket  
Discrete element method

### ABSTRACT

In this paper, a Discrete Element Method (DEM) for the evaluation of the effective thermal conductivity of pebble beds in fusion blankets is presented. Pebble beds are multiphase materials in which both the solid and the gas phase filling the voids between particles coexist. The effective thermal conductivity of a pebble bed depends on the thermal properties of the two phases as well as on the system properties (e.g. gas pressure, temperature etc.). In particular, the pressure of the system is a key parameter for the heat transfer in a packed granular assembly since the thermal conductivity of a confined gas decreases with decreasing pressure (known as Smoluchowski effect). In this work, the influence of the gas pressure on the effective thermal conductivity in the Knudsen domain was implemented, to our knowledge, for the first time in a DEM code. The heat transfer mechanisms implemented are: when two particles touch each other the conduction through the contact area between them and, in any case, the conduction through the gas phase in the gap between neighbouring solid particles, may they be touching or not. These mechanisms are expected to dominate the heat transfer in a fusion breeder packed bed. Parametric studies were carried out to investigate the influence of the solid and gas materials, temperature, pressure and compression state. Numerical results were compared with existing experimental literature data and recent experiments carried out at Karlsruhe Institute of Technology (KIT).

### 1. Introduction

The breeder blanket is a key component of fusion reactors in which both tritium and heat are generated. In order to ensure tritium release and heat recovery adequate thermal properties of the breeder zone are required [1,2]. In the solid breeder blanket concept the breeder and the neutron multiplier are both in form of packed-pebble beds. Therefore, the thermal properties of the breeder zone are strictly related to the thermal properties of the packed pebbles. Due to their discrete nature, pebble beds show a complex fully coupled thermomechanical behaviour. In a constrained bed, the thermal expansion and the irradiation-induced swelling of each single particle generate stresses that in turn have an impact on the packed state, on the heat exchange between pebbles and thus on the effective thermal conductivity of the bed. Pebble beds are multiphase materials consisting of a solid phase (pebbles) and a gas phase (interstitial purge gas for tritium extraction). The solid phase forms the skeleton of the bed while the gas phase constitutes the filling matrix between pebbles. A variation of the skeleton or matrix material as well as the system conditions (e.g. temperature and gas pressure) can strongly influence the effective thermal conductivity.

The aim of this work is the evaluation of the effective thermal conductivity of packed granular assemblies for different skeleton-matrix combinations, system conditions and compression states. To this end an in-house thermal-DEM code was developed. A 3D network model was implemented to determine the heat exchange in packed systems under an imposed thermal gradient. The particle interconnection is defined by thermal resistors to simulate the resistance to the heat transfer between two contacting particles in function of the thermal contact type. In particular, by implementing the theory developed by Batchelor and O'Brien [3] two main types of contact are defined: particles touching each other or with a separation gap. In order to simulate the influence of the gas pressure on the heat transfer in a packed bed, the Smoluchowski effect [4] was further introduced in the present thermal contact conductance model. The Smoluchowski effect accounts for the reduction of the gas thermal conductivity with its pressure when the gas is confined in small gaps as in a packed bed. In literature, several studies about the influence of the gas pressure on the effective thermal conductivity in packed granular system exist [5–7]. The typical S-shaped curve, characteristic of the Smoluchowski effect, was successfully reproduced by both experiments [5,7] and phenomenological

\* Corresponding author.

E-mail address: [marigrazia.moscardini@kit.edu](mailto:marigrazia.moscardini@kit.edu) (M. Moscardini).

models [6,7]. To explicitly model Smoluchowski effect at the scale of contacting pebbles, the pressure-dependent gap conduction has been recently modelled using the finite element method [8]. Nevertheless, this work represents an innovative step in the DEM community being the first investigation in which the influence of the gas pressure on the heat transfer was implemented in a DEM code.

In a packed bed, several heat transfer mechanisms take place: conduction within the solid material, conduction through the contact area between touching particles, conduction in the gas phase, gas convection and radiation between particles. In this work the first three mechanisms were considered, which are expected to dominate the heat transfer in a fusion breeder packed bed. The heat radiation contribution increases with the particle temperature and size [9], while it reduces with the increase of the bed density [10]. A high packing factor increases the absorption of radiation in the packed structure reducing the radiative bed density [10]. It has been reported that the thermal radiation in packed beds is negligible for particles with a diameter less than 1 mm in the temperature range of 0–1440 °C [9]. In the same study, the contribution of thermal radiation was found to be appreciable above 400 and 150 °C for particles with a diameter of 10 and 100 mm, respectively. In [11] the contribution of the thermal radiation was found to be negligible below 130 °C for graphite spheres of 60 mm in diameter with an average PF of 61%. Thus, neglecting thermal radiation is justified here due to the small particle size and the high packing factor of the studied assemblies.

The code was validated by comparison with existing experimental literature data and recent experiments carried out in KIT [12]. Parametric studies were carried out to investigate the influence of both skeleton and matrix materials, temperature, the compressive state of the bed as well as the interstitial pressure.

In this paper, the developed 3D thermal network model is presented in Section 2. Parametric sensitivity studies and the comparisons with existing experimental results are discussed in Section 3. Finally, in Section 4, the conclusions are reported.

## 2. 3D thermal network model

In this work the 3D thermal network model based on the theory proposed in [3] and later used in [13,14] was implemented to evaluate the effective thermal conductivity of a packed granular system. The model was further extended to include the influence of the interstitial gas pressure and temperature, by including the Knudsen number in the thermal contact conductance model. This decisive step allows to study, for the first time by means of DEM code, the influence of the interstitial gas pressure on the heat transfer and thus on the effective thermal conductivity in the gas flow transition region named Knudsen domain.

### 2.1. Global thermal model

To investigate the heat transfer in a granular system, with the main aim to determine the effective thermal conductivity of the assembly, an in-house thermal-DEM code was developed.

A 3D thermal resistor network model was implemented to determine the heat exchange in packed systems under an imposed thermal gradient. Monosized and polydispersed packed granular systems were generated by means of a modified version of the Random Close Packing (RCP) algorithm described in [15,16]. The RCP presented in [15,16] generates assemblies of packed spheres in periodic configuration. With the implementation of periodic boundary conditions (PBCs), the generated assemblies represent the bulk region of the pebble beds. In order to apply a thermal gradient along the height of the assemblies, the RCP was slightly modified [17]. The PBCs in the upper and bottom boundaries were replaced by rigid walls. As thoroughly explained in [17], during the iterations the desired packing factor is approached reducing the radius of the spheres. The diameter of the particles is equal to the desired value only if the objective packing factor is reached. Otherwise

if a slight variation between the objective and the obtained PF occurs, the radius of the particles is scaled to match the objective PF with the desired particle size. In a granular system two phases coexist. Pebbles as a whole identify the solid phase composing the skeleton of the system, while the interstitial gas represents the matrix of the system. In the proposed thermal contact conductance model the pebbles are interconnected by thermal resistors defined by the different type of thermal contact. The heat  $q_{ij}$  transferred between the two particles  $i$  and  $j$  is

$$q_{ij} = C_{ij}^{eff} (T_i - T_j). \quad (1)$$

Here,  $T_i$  and  $T_j$  are the temperatures of particle  $i$  and  $j$ , respectively. An individual temperature is assigned to each particle.  $C_{ij}^{eff}$  [W/K] is the local effective conductance, which is related to the type of the thermal contact as thoroughly described in Section 2.2. Then,  $q_{ij}$  [W] is evaluated at each time step for each contact in the whole assembly. The rate of temperature change  $\dot{T}_i$  of the  $i$ -th pebble is updated as

$$\dot{T}_i = \sum_j \frac{q_{ij}}{m_i c_p}, \quad (2)$$

where  $m_i$  [Kg] and  $c_p$  [J/Kg K] are the mass and the heat capacity of the solid material, respectively. For an imposed thermal gradient, the calculation ends when the assembly reaches the steady state configuration according to

$$\frac{\sum_i m_i c_p T_i^n - \sum_i m_i c_p T_i^{n-1}}{\sum_i m_i c_p T_i^{n-1}} < \text{TOL}, \quad (3)$$

where TOL is set to  $10^{-10}$  in the present work for a typical time steps of  $\sim 0.01$ – $1$  s. Eq. (3) represents the variation of the thermal energy in the assembly between two consecutive iterations. The thermal diffusion time defined as

$$\delta t = \frac{\rho c_p R_{min}^2 \tau^2}{k_s} \quad (4)$$

determines the time step required to achieve the solution for the explicit scheme used in the simulation [18]. Here, the ratio  $\left(\frac{\rho c_p}{k_s}\right)^{-1}$  [ $\text{m}^2/\text{s}$ ] represents the thermal diffusivity of the solid material, which determines the heat transfer rate in the particles.  $\rho$  [ $\text{kg}/\text{m}^3$ ] and  $k_s$  [ $\text{W}/\text{mK}$ ] are the density and the thermal conductivity of the solid material, respectively. The minimum thermal diffusion time in the assembly is defined by dividing the square of the minimum radius in the assembly  $R_{min}^2$  [ $\text{m}^2$ ] by the thermal diffusivity of the solid material. The parameter  $\tau$  [–] is introduced to ensure stability of the calculation for several conditions (e.g. different gas pressure, gas type, solid materials, radius of the particles etc.). A value of  $\tau = 0.5$  ensured the stability and the convergence of the simulations in every condition. However, under certain conditions such as low gas pressure or small pebble diameters  $\tau = 0.5$  turned out to be too restrictive resulting in a high computational time. In these circumstances  $\tau$  can be increased (e.g. to 1, 2, 4) until the convergence is assured to reduce the computational time. If the convergence is achieved, the variation of this parameter does not affect the results of the simulation. Once that the steady state configuration is reached, the effective thermal conductivity of the assembly is evaluated as

$$k_{eff} = \frac{\sum_i q_{i,bw} H}{A(T_{top} - T_{bottom})}, \quad (5)$$

where  $\sum_i q_{i,bw}$  [W] is the total heat transferred between pebbles and the bottom wall.  $H$  [m] and  $A$  [ $\text{m}^2$ ] are the height and the cross sectional area of the assembly, respectively.  $T_{top} - T_{bottom}$  is the imposed thermal gradient between the top and the bottom wall, set to 1K in this work.

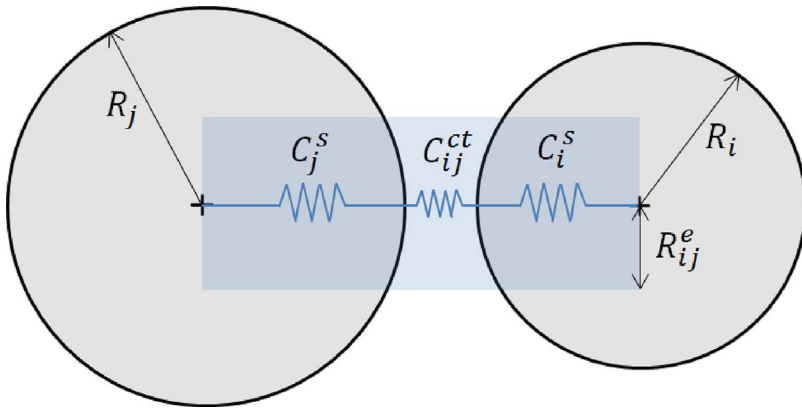


Fig 1. Contacts defined as a series circuit of three resistors: solid-contact-solid.

2.2. Effective thermal contact conductance

In the 3D thermal network, each contact is defined as a series circuit consisting of three resistors. As exemplarily shown in Fig. 1, the three resistors represent the resistance to the heat transfer in the two solid particles and in the thermal contact region. The respective thermal conductances are namely  $C_i^s$ ,  $C_j^s$  and  $C_{ij}^{ct}$  [W/°C]. This basic configuration defines the local effective thermal conductance of the contact pair as

$$C_{ij}^{eff} = \left[ \frac{1}{C_i^s} + \frac{1}{C_{ij}^{ct}} + \frac{1}{C_j^s} \right]^{-1} \tag{6}$$

To evaluate  $C_i^s$ ,  $C_j^s$  and  $C_{ij}^{ct}$ , the theoretical derivation developed in [3] and applied in [13,14] was adopted.

The thermal contact is assumed to be a contact area between touching particles (Fig. 2-a) or a separation gap (Fig. 2-b). When the distance between the centers of the two particles  $D_{ij}$  [m] is greater than the sum of their radii, the thermal contact is defined as a separation gap with a characteristic distance of

$$h_{ij} = D_{ij} - (R_i + R_j). \tag{7}$$

Otherwise, according to Hertzian contact theory, a contact area defined by a contact radius as

$$r_c = \sqrt{|h_{ij}| \frac{R_{ij}}{2}}. \tag{8}$$

between the two pebbles exists. Here,  $R_{ij} = \frac{2R_i R_j}{R_i + R_j}$  [m] is the equivalent radius. Thermal contact pairs are included in the computation if  $h_{ij} < \epsilon R_{ij}$ , where  $\epsilon$  is the cut-off range limit. In the present work a value of 0.5 was adopted according to [13,14].

Batchelor et al. [3] demonstrated analytically that the heat transport between two spheres mainly occurs across the particle surface

closest to the contact region, where the contact region can be either a contact area or a separation gap. It is therein assumed that the heat is transferred through a cylindrical zone of radius  $R_{ij}^e = \chi R_{ij}$  [m], as shown in Fig. 1. The axis of the cylinder is aligned with the centers of the two particles and the effective radius  $R_{ij}^e$  is defined as a fraction  $\chi$  [ / ] of the equivalent radius  $R_{ij}$ .  $\chi$  gives the fraction of the sphere curvature involved in the heat transport. In literature this parameter is set to match experimental [13] or numerical [14] results carried out by other numerical tools. This parameter strongly influences the results of the DEM simulation, thus an initial calibration of the code was performed, see Section 3.

According to Batchelor and O'Brien [3]  $C_i^s$ ,  $C_j^s$  and  $C_{ij}^{ct}$  are evaluated as:

- a. Conductance of the solid particles

$$C_n^s = \pi k_s \frac{R_{ij}^e{}^2}{R_n}, \quad n = i \text{ or } j \tag{9}$$

- b. Conductance of the thermal contact

$$\text{contact area between touching particles: } C_{ij}^{ct} = \begin{cases} \pi k_g R_{ij} \left[ \frac{2\eta_{ij}}{\pi} - 2 \ln \eta_{ij} + \ln \alpha^2 \right] & \text{if } \eta_{ij} > 100 \\ \pi k_g R_{ij} [0.22\eta_{ij}^2 - 0.05\eta_{ij} + \ln \alpha^2] & \text{if } \eta_{ij} < 1 \\ \text{linear interpolation} & \text{otherwise} \end{cases} \tag{10}$$

$$\text{separationgap: } C_{ij}^{ct} = \begin{cases} \pi k_g R_{ij} \ln \alpha^2 & \text{if } \xi_{ij} < 0.1 \\ \pi k_g R_{ij} \ln \left[ 1 + \frac{R_{ij}^e{}^2}{R_{ij} h_{ij}} \right] & \text{otherwise} \end{cases} \tag{11}$$

Here,  $k_g$  [W/mK] and  $\alpha = k_s/k_g$  [ / ] are the thermal conductivity of the interstitial gas and the solid to gas thermal conductivity ratio, respectively.  $\eta_{ij} = \alpha r_c / R_{ij}$  [ / ] and  $\xi_{ij} = \alpha^2 h_{ij} / R_{ij}$  [ / ] are two non-dimensional parameters defining the conductance in the contact area and in the

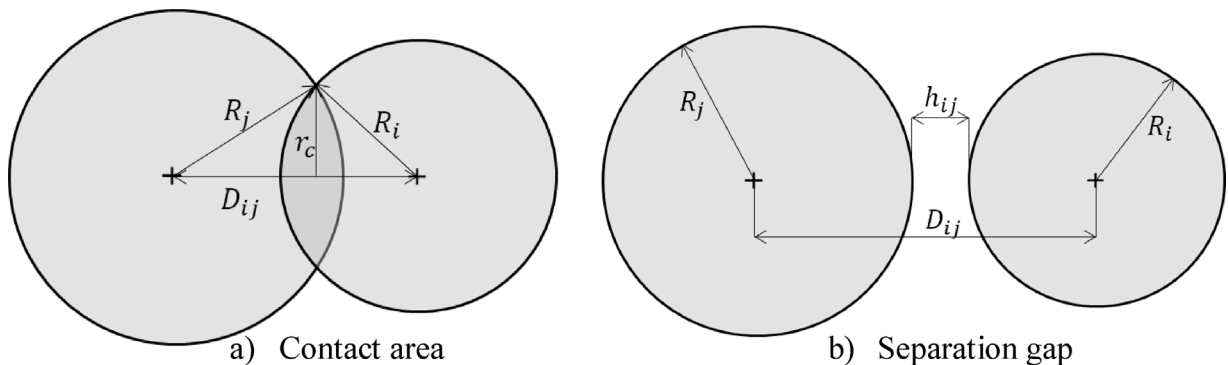


Fig. 2. Types of thermal contact regions: a) Contact area for touching particles, b) Separation gap for particles nearly in contact.

separation gap, respectively. The cut-off values for  $\eta_{ij}$  and  $\xi_{ij}$  reported in Eqs. (10) and (11) were estimated according to [3]. A further and innovative step introduced in this work is the implementation of the influence of the gas pressure, i.e. the Smoluchowski effect, on the heat transfer in a DEM code. To this end the theory of Batchelor and O'Brien [3], where only uniform thermal properties of interstitial gas were used, was modified as reported in the following section.

### 2.3. Implementation of the Smoluchowski effect

For an unconfined gas the thermal conductivity is independent of its pressure, while it decreases with decreasing pressure when the gas is confined in small gaps, as in a packed bed. This is the so-called Smoluchowski effect [4]. In particular, the thermal conductivity of a gas is independent of its pressure as long as the mean free path of the gas molecule is much smaller than dimensions of the space where it is confined. At a given temperature, since the mean free path is inversely proportional to the gas pressure, when the pressure decreases the mean free path gradually increases reaching the order of magnitude of the confining dimension. In turn the interaction between the gas molecules becomes more sporadic and the heat is mainly transferred by interaction of the gas molecule with the walls. As a consequence, the gas thermal conductivity becomes strongly dependent on the gas pressure. The Knudsen number ( $K_n = \Lambda/L$ ) is representative of the likelihood of the molecule interactions thus of the degree of rarefaction of a gas as will be discussed below. Here  $\Lambda$  [m] and  $L$  [m] are the mean free path and the geometrical dimension of the confining space, respectively. Note that for a packed granular system, the dimension of the confining space ( $L$ ) is ill-defined, since the topological features of the pore space contains gap sizes ranging from almost zero to the magnitude of the pebble size. However, the effective value  $K_n$  can be defined for each individual contact, depending on the geometry of the contact region. When  $K_n$  increases the probability of interaction between gas molecules decreases until to be neglected, which defines the three following gas regimes:

- Continuum regime: For  $K_n < 0.001$  the heat in the gas is transferred by molecular interactions and the gas thermal conductivity as well as the thermal conductivity of the packed granular system is independent of the gas pressure. This is defined as the continuum regime, where the gas thermal conductivity is equal to its bulk value.
- Transition regime: For  $0.001 < K_n < 10$  the gas thermal conductivity and thus the effective thermal conductivity of the granular assembly drop as the gas pressure decreases. Decreasing the gas pressure the effective thermal conductivity of the bed drops because the mean free path gradually reaches the order of magnitude of the characteristic dimension of the volume where it is enclosed and the thermal transfer in the gas became less effective.
- Free molecule regime: For  $K_n > 10$  (very rarefied gas) the collision between molecules can be neglected, the thermal energy is transferred directly by the interactions of the gas molecule with the confining surfaces. This regime is called free molecule regime, the thermal conductivity of the gas and thus the effective thermal conductivity of the assembly are low and again are independent on the gas pressure.

The combination of these three regimes provides the well-known S-shape curve while plotting the effective conductivity of the packed bed with respect to the gas pressure. Kaganer [19] proposed a correlation for the estimation of the thermal conductivity  $k_g^c$  of a confined gas as a function of the Knudsen number as

$$k_g^c = \frac{k_g}{1 + 2\beta K_n}, \quad (12)$$

with

$$K_n = \frac{\Lambda}{L} = \frac{\mathcal{K}T}{\sqrt{2}\pi d_m^2 PL}. \quad (13)$$

Here,  $\mathcal{K} = 1.38 \cdot 10^{-23}$  [J/K] is the Boltzmann constant,  $T$  [K] is the temperature,  $d_m$  [m] is the kinetic molecule diameter and  $P$  [Pa] is the gas pressure. Furthermore,  $k_g$  [W/m K] is the bulk thermal conductivity of the interstitial gas and  $\beta$  [1] represents the amount of energy transfer between the gas molecule and the solid material. It depends on the gas type, the solid material and the temperature of the system. Different correlations were proposed for the estimation of  $\beta$ . In this work, the correlation proposed by Wakao and Kagnei [20] was used:

$$\beta = \frac{2 - \alpha_c}{\alpha_c}. \quad (14)$$

Here the thermal accommodation coefficient  $\alpha_c$  [1] represents the effectiveness of the energy transfer between molecule and wall. It depends on the two phases composing the assembly as well as on the gas temperature. In this work the correlation derived by Boule [21] and later modified by Goodman [22] was used

$$\alpha_c = \frac{Cm_r}{(1 + m_r)^2}, \quad (15)$$

where  $m_r = m_g/m_s$  [1] is the ratio of the gas ( $m_g$ ) to solid ( $m_s$ ) atomic masses [g/mol]. Here,  $C = 2.4$  [1] is an empirical constant introduced by Goodman to better reproduce the experimental results. Eq. (15) reduces to the Boule formula for  $C = 0$ . The theory of Batchelor and O'Brien [3], described above, was here slightly modified to implement the Smoluchowski effect. To this end  $k_g$  was substituted with  $k_g^c$  [W/m K] in the Eqs. (10) and (11) and in the parameter  $\alpha$ . This innovative step allows taking into account the reduction of the gas thermal conductivity due to the reduction of the gas pressure. Plugging the Knudsen number, previously defined in Eq. (12) as  $\Lambda/L$ ,  $k_g^c$  becomes

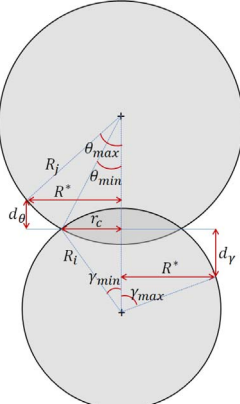
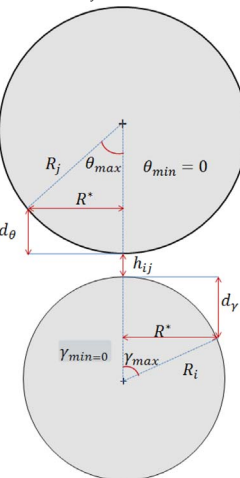
$$k_g^c = \frac{k_g}{1 + 2\beta \left( \frac{\Lambda}{d_{ave} + h_{ij}} \right)} \quad (16)$$

For each contact, the geometrical dimension  $L$  is replaced by the mean gap size  $d_{ave} + h_{ij}$ . When  $h_{ij} < 0$ , the thermal conductance is evaluated according to Eq. (10) (contact area between touching particles) and  $h_{ij}$  in Eq. (16) is set equal to 0, otherwise, i.e. for  $h_{ij} > 0$ , Eq. (11) (separation gap) is used. The evaluation of  $d_{ave}$  is based on the contact configurations reported in Table 1 and in Table 2. The two tables refer to the particle–particle and the particle-wall contacts, respectively. In the Batchelor and O'Brien theory [3], the contribution of the gas conduction in the zone nearby the contact area or in the separation gap ( $h_{ij}$ ), is taken into account in the heat transport. The cylindrical zone, with radius  $R_{ij}^c = \chi R_{ij}$ , defines the fraction of the sphere curvature involved in the heat transport. Therefore,  $d_{ave}$  is the sum of the integrated distances  $\bar{d}_\gamma$  and  $\bar{d}_\theta$  over the specified portions of the sphere surface.

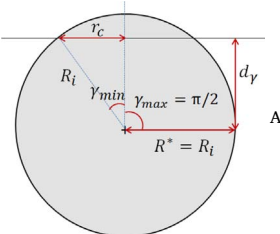
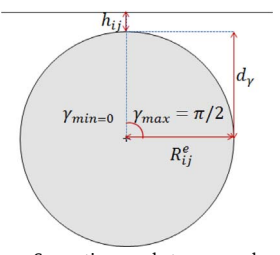
### 3. Code calibration and validation

In the following sections the simulations carried out with the KIT thermal-DEM code introduced above are presented. In Section 3.1 the code calibration is reported. The parameter  $\chi$  was set to match the experimental results carried out in KIT [12]. Then, with the selected  $\chi$ , several simulations were run to validate the code under different system conditions and with different materials. In particular, in Sections 3.2, 3.3 and 3.4 the experimental results obtained in [12] were reproduced varying the gas type, the gas pressure and the compression state, respectively. Finally, in Section 3.5 the comparison between numerical and experimental literature results for different solid breeder materials is reported. The physical characteristics of the studied solid materials and gases are summarized in Tables 3 and 4, respectively. In Table 3 the densities of the ceramic materials are given as function of the porosity

**Table 1**  
Evaluation of the gap size  $d_{ave}$  for the two different configurations between two spheres.

Geometrical configuration of the contact	$d_{ave}$
 <p>Two spheres touching at a contact area of radius <math>r_c</math> (<math>R_i &lt; R_j</math>)</p>	$\gamma_{min} < \gamma < \gamma_{max}; \theta_{min} < \theta < \theta_{max}$ $\gamma_{max} = \sin^{-1}(R^*/R_i); \theta_{max} = \sin^{-1}(R^*/R_j)$ $\gamma_{min} = \sin^{-1}(r_c/R_i); \theta_{min} = \sin^{-1}(r_c/R_j)$ <p>if <math>R_i &lt; R_{ij}^e R^* = R_i</math> otherwise <math>R^* = R_{ij}^e</math></p> $\bar{d}_\gamma = \frac{\int_{\gamma_{min}}^{\gamma_{max}} R_i(1 - \cos \gamma) d\gamma}{\int_{\gamma_{min}}^{\gamma_{max}} d\gamma}$ $\bar{d}_\theta = \frac{\int_{\theta_{min}}^{\theta_{max}} R_j(1 - \cos \theta) d\theta}{\int_{\theta_{min}}^{\theta_{max}} d\theta}$ $d_{ave} = \bar{d}_\gamma + \bar{d}_\theta$
 <p>separation gap between two spheres (<math>R_i &lt; R_j</math>)</p>	<p>As for the above case of two touching spheres with the exception of the following changes:</p> $0 < \gamma < \gamma_{max}; 0 < \theta < \theta_{max}$ $r_c = 0$ $d_{ave} = \bar{d}_\gamma + \bar{d}_\theta$

**Table 2**  
Evaluation of the gap size  $d_{ave}$  for the two different configurations of a contact between a sphere and a wall.

Geometrical configuration of the contact	$d_{ave}$
 <p>sphere touching a wall at a contact area of radius <math>r_c</math> (<math>R_j \rightarrow \infty</math>)</p>	$\gamma_{min} < \gamma < \pi/2 \quad \gamma_{min} = \sin^{-1}(r_c/R_i)$ $d_{ave} = \bar{d}_\gamma = \frac{\int_{\gamma_{min}}^{\pi/2} R_i(1 - \cos \gamma) d\gamma}{\int_{\gamma_{min}}^{\pi/2} d\gamma}$
 <p>Separation gap between a sphere and a wall (<math>R_j \rightarrow \infty</math>)</p>	<p>The wall is considered as a sphere with an infinite radius, thus <math>\bar{d}_\theta</math> approaches zero.</p> <p>As for the above case of a spheres touching a wall with the exception of the following changes:</p> $0 < \gamma < \pi/2$ $r_c = 0$ $d_{ave} = \bar{d}_\gamma$

p. The thermal conductivities of the solid and gas materials were evaluated, by means of the correlation reported in Table 3 and in Table 4, at the investigated temperature of each simulation. With application to breeder beds, several experimental campaigns have been carried out to characterize the thermal properties of the various ceramic breeder material candidates. In literature different correlations for the estimation of  $k_g$  and  $c_p$  for the same breeding material are reported [23]. In this work, the influence of the thermal conductivity of the solid material on the effective thermal conductivity was investigated. For the EU reference material (EU Ref.) the most recent and reliable thermal conductivity values were considered [24]. They refer to a porosity of ~11%, while the pebbles used in the experiments [12] have a porosity of around 6%.

In Section 3.5 the investigation of other two other solid breeder materials  $Li_2TiO_3$  and  $Li_2ZrO_3$  is reported. The simulations with  $Li_2TiO_3$  pebbles were carried out implementing the correlations reported in [26] and [27]. In this work both monosized and polydispersed assemblies were studied. In Fig. 3 the pebble size distribution used in the experiments carried out in KIT [12] is reported together with the produced assembly used for the numerical simulations. All assemblies consist in 5000 perfect spherical particles packed in virtual box using a

Random Close Packing (RCP) algorithm. The height of the assemblies was set to 20 mm while the dimension of the square cross section of the assemblies was evaluated as a function of pebble size and packing factor as  $l^2 = \frac{V_{tot,s}}{H PF}$ . Here,  $V_{tot,s}$  and  $H$  are the total volume of the spheres and the height of the assembly, respectively.

In Sections 3.1, 3.2, 3.3 and 3.4 when the compression state is not specified the reported results are the average value between uncompressed and compressed bed at 6 MPa in agreement with [12]. In [12] to obtain a well-defined mechanical state of the bed a mechanical conditioning of three loading/unloading cycles up to 6 MPa was applied. The existing mechanical KIT DEM code [15,16,32] was used to simulate the mechanical compression. The mechanical DEM code was successfully used in previous studies [15,16,32] to investigate the mechanical behaviour of monosized, binary and polydispersed pebble assemblies. In Fig. 4 the simulation of the first four compressive loading-unloading cycles is reported. After the first unloading a large residual strain is observed, while in the consecutive cycle it is strongly reduced indicating in a lower additional compaction of the bed. In view of this finding, the second loading cycle was considered representative of a compressed bed in the simulations.

### 3.1. Influence of $\chi$ parameter and code calibration

The parameter  $\chi$  influences the value of the effective thermal conductivity since it determines the effective radius of the cylindrical zone involved in the heat transfer (Fig. 1). In literature  $\chi$  is chosen to match experimental or analytical results. In Fig. 5 the comparison between experimental and numerical results varying  $\chi$  is reported, where  $\chi$  was varied in the range 0.6–0.8 to study its influence on the bed’s thermal conductivity. Numerical simulations and experiments were carried out with pebbles of EU Ref. in helium at ~64.2% packing factor with the polydispersion reported in Fig. 3. As shown in the figure, the effective thermal conductivity decreases with decreasing  $\chi$  according to the reduction of the fraction of the sphere surface considered for the heat transport. Nevertheless, the variation of  $\chi$  does not change significantly

**Table 3**  
Physical characteristics of the used solid materials.

Material	Parameter	Value
EU Ref. (Li <sub>4</sub> SiO <sub>4</sub> + 10 mol% Li <sub>2</sub> SiO <sub>3</sub> )	$k_s$ [W/m K]	Correlation fitting the values reported in [24] with 89%TD (Theoretical Density): $7.317 \times 10^{-12}T^4 - 1.302 \times 10^{-8}T^3 + 8.712 \times 10^{-6}T^2 - 0.002876T + 2.62$ ; T in °C
	[J/Kg K]	$(-5.33 \times 10^{-7}T^2 + 0.001925T + 1.238) \times 1000$ [25]; T in °C
	$c_p$	
	$\rho$ [kg/m <sup>3</sup> ]	$2400(1 - p)$ ; $p = 0.05$
	$m_s$ [g/mol]	119.85
Li <sub>2</sub> TiO <sub>3</sub>	$k_s$ [W/m K]	$[(1 - p)^{2.9}(5.35 - 4.78 \times 10^{-3}T + 2.87 \times 10^{-6}T^2)$ [26], T in K $[(1 - p)/(1 + (1.06 - 2.88 \times 10^{-4}T)p)](4.77 - (5.11 \times 10^{-3}T) + (3.12 \times 10^{-6}T^2))$ [27]; T in K
	$c_p$ [J/Kg K]	$355(T - 100)^{1.1}/(1 + (0.37T^{1.05}))$ [26]; T in K $(0.73 + (8.44 \times 10^{-4}T) - (1.67 \times 10^{-7}T)) \times 1000$ [27]; T in K
	$\rho$ [kg/m <sup>3</sup> ]	$3430(1 - p)$ ; $p \sim 0.08$
	$m_s$ [g/mol]	109.76
	$k_s$ [W/m K]	$(1 - p)^{5/3}[(3.643/(1 + 0.00155T)) + 7.579 \times 10^{-10}T^3]$ [28]; with T in K
Li <sub>2</sub> ZrO <sub>3</sub>	$c_p$ [J/Kg K]	$(1.022 - (3.696 \times 10^{-5}T) - (2.791 \times 10^{-4}T^{-2})) \times 1000$ [29]; with T in K
	$\rho$ [kg/m <sup>3</sup> ]	$4150(1 - p)$ ; $p = 0.2$
	$m_s$ [g/mol]	153.1

**Table 4**  
Physical characteristics of the used gas types.

Material	Parameter	Value
Helium	$k_g$ [W/mK]	$3.366 \times 10^{-3}T^{0.668}$ [23]; T in K.
	$d_m$ [m]	$2.15e - 10$ [30]
	$m_g$ [g/mol]	4
Air	$k_g$ [W/m K]	Correlation fitting the values reported in [31]: $-1 \times 10^{-11}T^3 - 4 \times 10^{-8}T^2 + 8 \times 10^{-3}T + 0.0241$ ; T in °C
	$d_m$ [m]	$3.66e - 10$ [30]
	$m_g$ [g/mol]	28.96

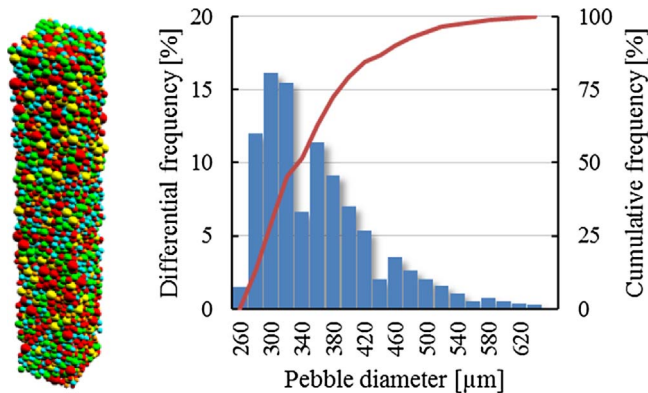


Fig. 3. (a) Assembly generated with the size distribution of EU Ref. [12], different colours represent different ranges of pebble sizes; (b) size distribution of EU Ref. [12].

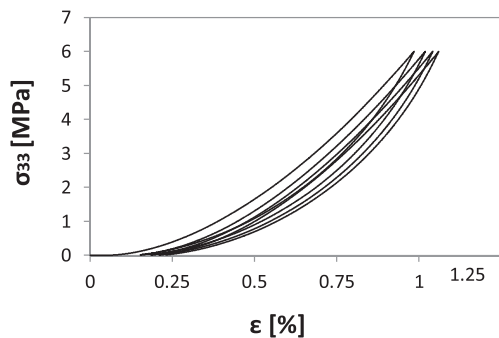


Fig. 4. Uniaxial compression loading cycles.

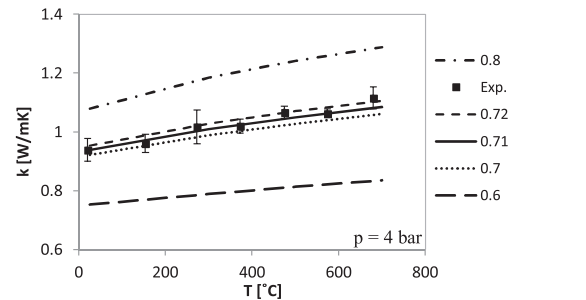


Fig. 5. Influence of the  $\chi$  parameter on the effective thermal conductivity (polydispersed assembly of EU Ref. in helium) and comparison with experimental results [12].

the trend of the effective thermal conductivity vs. the temperature, shifting the curve to higher or lower values with the reduction or increase of  $\chi$ , respectively. For a given  $\chi$  value, the temperature-dependent behaviour is brought from the value of  $k_s$  and  $k_g^c$  at the investigated temperature, quantitatively matching the experimental results of the effective thermal conductivity without additional fitting. In this work a value of 0.71 was used to match the experimental results performed in KIT [12]. Note that in the present study  $\chi$  is set only once in order to calibrate the code and then kept fixed for all the other simulations (e.g. different solid materials, gas pressures/type and compression state). The choice of  $\chi$  may differ for systems with different sized particles, however due to the limited available data, we use  $\chi = 0.71$  in this paper for a size range from 0.25 to 1.9 mm, corresponding to experimental data from various sources [12,37,38], which is the relevant size range in fusion applications.

### 3.2. Influence of the gas type

In this section the influence of the gas type on the effective thermal conductivity was numerically investigated. Numerical simulations were

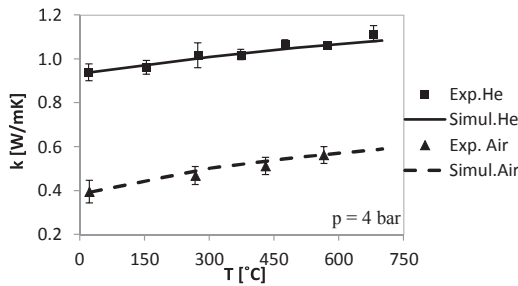


Fig. 6. Comparison between numerical and experimental results for polydispersed assembly of EU Ref. pebbles in air and He.

carried out with the above mentioned polydispersed assembly of EU Ref. in helium and air at 4 bar. The investigated temperature range between room temperature and 700 °C is consistent with the expected operating temperature range of the ceramic breeder material and the experiments conducted in [12].

In Fig. 6 the comparison between numerical and experimental results is reported.

A good agreement with the experimental outcomes is observed. The DEM simulations accurately capture the different thermal behaviour of the granular assembly in helium and air. An increase of the effective thermal conductivity with the temperature was found for all investigated compositions in both atmospheres in agreement with experimental observations. As experimentally observed, a pebble bed in air shows a reduction of the effective thermal conductivity of about 45–55% compared to simulation for helium. This difference is determined by the different thermal conductivities of the two gases. In particular, in the considered temperature range the thermal conductivity of unconfined helium is about five times higher than the thermal conductivity of unconfined air.

### 3.3. Influence of the gas pressure

In this section, the influence of the gas pressure on the effective thermal conductivity of pebble beds is analyzed. Simulations were carried out with the above mentioned polydispersed assembly of EU Ref. In Fig. 7 the comparison between numerical simulations and experimental results reported in [12] is shown.

The experimental results refer to the average value between compressed and uncompressed bed of EU Ref. in helium at 1.2, 2 and 4 bar as expressed by the correlations reported in [12]. In the simulation the gas pressure was varied in the range 0.0001–10 bar to cover all the gas regimes. Moreover the simulations results are reported for compressed (6 MPa) and uncompressed beds to show the influence of the compressive state at different gas pressure. The S-shape curve characteristic of the Smoluchowski effect is reproduced, meaning that the continuum, transition and free molecule gas regimes are numerically obtained. In the pressure range between 1 and 4 bar a good agreement with experimental outcomes was found. In this pressure range, both theoretical (according to Eqs. (12) and (13) and experimental results show an increasing of the effective thermal conductivity of the bed with the gas

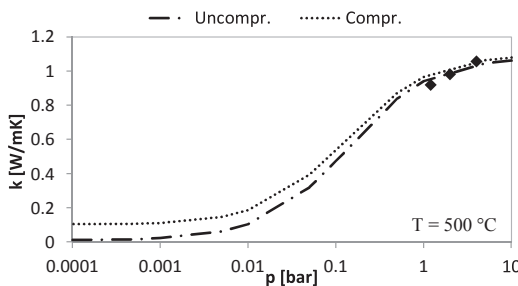


Fig. 7. Influence of the pressure for assemblies with different compression states.

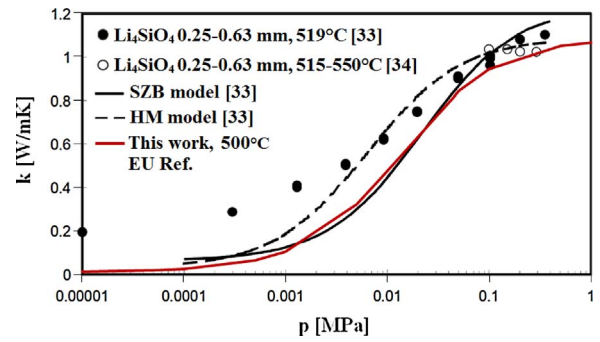


Fig. 8. Comparison between effective thermal conductivities reported in literature and numerical DEM results obtained in this work (after [33]).

pressure. The effective thermal conductivity increases up to ~5 bar, then a limited pressure dependence is observed. This indicates that, in the range 1–5 bar, the filling gas is in the upper part of the transition region. The influence of the compressive load was found to be more pronounced at very low pressures (free molecule regime) decreasing with the increase of the pressure in the transition regime to almost vanishing difference in the continuum regime where the breeder beds are supposed to operate. The DEM results are compared with literature data in Fig. 8. The results reported in [33] cover the low gas pressure range down to 0.0001 MPa, while in [34] experiments were conducted in the pressure range 0.1–0.3 MPa. The figure is reproduced from [33] where the experimental results were also compared with the correlations derived by Bauer and Schlünder (SBZ) [35] and Hall and Martin (HM) [36]. The numerical values obtained in this study are overlaid with a solid red line.

Both numerical and experimental results show a strong influence of the filling gas pressure in the pressure range 0.0001–0.1 MPa. The dependence on the helium pressure is drastically reduced, although still present, for pressures above 0.1 MPa. In contrast to the outcomes of [33] and of the present study, no influence of the helium pressure on the thermal conductivity of the pebble bed is found in [34]. For pressure above 0.05 MPa the numerical results are in good agreement with the experimental values obtained in [33]. The observed difference between the experimental and simulation values is less than 10%. Lower thermal conductivity values, especially between numerical simulations and experiments, were numerically obtained at lower gas pressures. The thermal radiation is not implemented in the present numerical model. Accounting for the thermal radiation, the effective thermal conductivity values are expected to slightly increase in the low pressures region where radiation is the predominant heat transfer mechanism. Due to the absence of uncertainty bands on the experimental results the consistency between experimental and numerical results cannot be assessed. A good agreement between numerical and SZB analytical results is obtained in the studied pressure range while, the HM model gives higher values.

In Figs. 9 and 10 the influence of gas type and temperature on the bed effective thermal conductivity as a function of the gas pressure is reported, respectively. The simulations were carried out for an uncompressed bed. The effective thermal conductivities reported in the figures are normalized with respect to the effective thermal conductivity evaluated at unconfined conditions.

For a given gas type and temperature, the thermal conductivity decreases with decreasing pressure showing the characteristic S-shaped curve. Compared to helium atmosphere, the onset of the transition regime is shifted to lower pressures in air. According to Eq. (13), in the transition regime both a lower kinetic diameter and a higher temperature result in a larger mean free path leading to a reduction of the gas contribution to the effective conductivity of the bed. The onset of the transition region is then shifted to lower pressures when the filling gas is characterized by a higher kinetic diameter  $d_m$  and when the bed

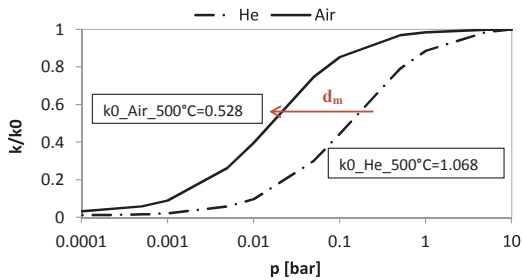


Fig. 9. Numerical results for polydispersed assembly in He and air normalized on unconfined values of thermal conductivity  $k_0$ .

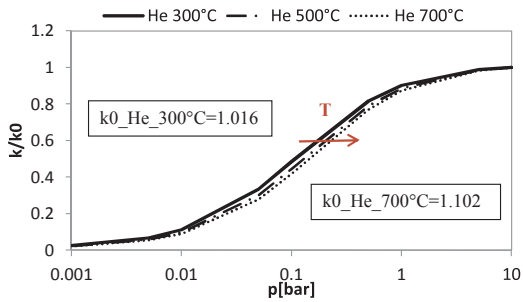


Fig. 10. Numerical results for polydispersed assembly in He at 300, 500 and 700 °C normalized on the values of thermal conductivity  $k_0$  under unconfined conditions.

temperature decreases, respectively.

### 3.4. Influence of the compressive load

The solid to gas thermal conductivity ratio  $k_s/k_g$  affects the heat transfer in the bed. In pebble beds with low  $k_s/k_g$  the heat flux is uniformly distributed among the solid and the gas phases, while in beds with a high ratio the heat flows mainly through pebbles and contact areas between particles since these are the paths of higher thermal conductivity. Therefore, the effective thermal conductivity of beds with high  $k_s/k_g$  ratios is influenced by the bed deformation. In particular, a compressive load acting on a breeder bed results in an increase of both the number of the contacts between pebbles and the contact area dimension of existing contacts. In Fig. 11, the numerical results on the effect of bed compression are compared with experimental results in [12].

The numerical results refer to the above mentioned polydispersed assembly of EU Ref. in helium and air at 4 bar in the temperature range of 25–700 °C for a compressed and an uncompressed state. In helium a good agreement with experimental values was obtained. The numerical

results in air slightly underestimate or overestimate the experiments for uncompressed and compressed state, respectively. However, considering the experimental uncertainty, a fairly good agreement with the experimental values was found also in air. An increase of the effective thermal conductivity with the applied compressive load was observed in both atmospheres. The influence of the compressive load was found to be more pronounced in air consistent with the higher  $k_s/k_g$  ratio than in helium, since the thermal conductivity of air is 5 times lower than that of helium. The increase of the thermal conductivity due to the compressive load was found to be more expressed at low temperatures with the tendency to vanish at high temperatures according to the decrease of the  $k_s/k_g$  ratio with the temperature.

### 3.5. Influence of the solid material

In order to further validate the KIT thermal-DEM code, experimental works reported in literature and referring to other breeding materials were numerically investigated. In particular, the effective thermal conductivity of  $\text{Li}_2\text{TiO}_3$  and  $\text{Li}_2\text{ZrO}_3$  pebble beds were studied. In Fig. 12 the numerical and experimental results reported in [37] for  $\text{Li}_2\text{ZrO}_3$  beds are compared to simulations. In [37]  $\text{Li}_2\text{ZrO}_3$  pebbles with a diameter of 1.2 mm at 63% packing fraction were investigated in helium atmosphere at 1 bar. The simulations were run with the same pebble size, packing state, gas type and pressure as used in the experiment [37]. The physical properties of  $\text{Li}_2\text{ZrO}_3$  used in the simulation are reported in Table 3. As shown in the figure the experimental results were reproduced. In particular, the nonlinear trend obtained in [37] was numerically obtained.

In Fig. 13 the comparison between experimental [38] and numerical results for  $\text{Li}_2\text{TiO}_3$  pebbles is reported. In the figure the experimental results are reported with diamonds while the simulations are represented by solid and dashed lines.

As indicated in Table 3, the simulations were carried out with the thermal properties  $k_g$  and  $c_p$  reported in [26] and additionally with the  $k_g$  and  $c_p$  values found in [27], respectively. In [38] the thermal conductivity of  $\text{Li}_2\text{TiO}_3$  pebble beds in helium gas at 1 bar was presented over the temperature range 400–800 °C. The experiments were carried out with 1.91 mm pebbles at 60% packing fraction. The same conditions were used to run the simulations. Due to the scattering of the experimental results both correlations used to estimate the thermal properties of the solid material give reasonable agreement when simulating the thermal conductivity of  $\text{Li}_2\text{TiO}_3$  beds. It is obvious from this graph that the correlations implemented to define the thermal properties of the solid material play a major role in the evaluation of the effective thermal conductivity of the bed. Nevertheless, a good agreement between numerical and experimental results was obtained.

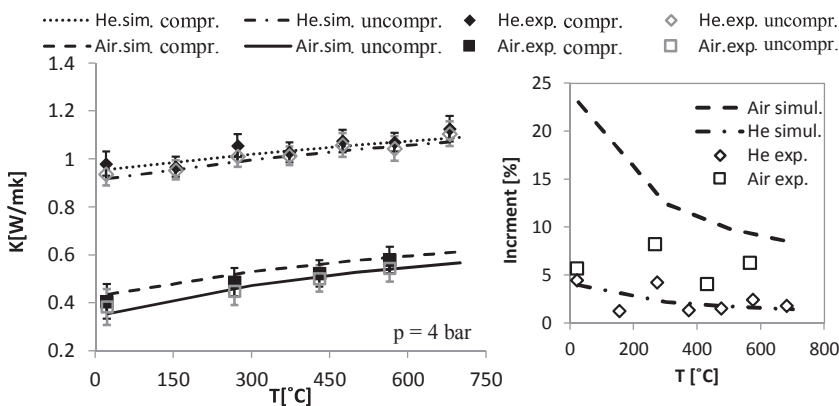


Fig. 11. Influence of the compressive load on the effective thermal conductivity for polydispersed assembly of EU Ref. pebbles in air and He.



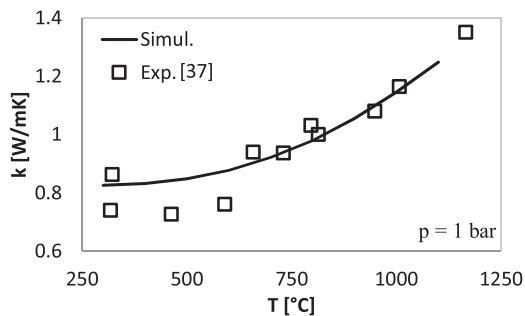


Fig. 12. Comparison between numerical simulation and experimental results [37] for  $\text{Li}_2\text{ZrO}_3$  pebbles in helium atmosphere.

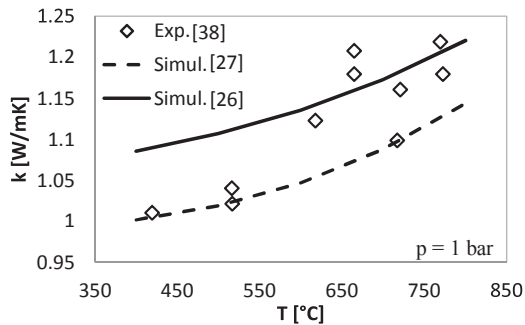


Fig. 13. Comparison between numerical simulations with thermal properties reported in [26] and [27] and experimental results according to [38] for  $\text{Li}_2\text{TiO}_3$  pebbles in helium atmosphere.

#### 4. Conclusion

In this work an in-house thermal-DEM code for the estimation of the effective thermal conductivity of packed spherical pebbles in stagnant fluid was presented. A 3D network resistor model was implemented to simulate the heat transfer between particles under an imposed thermal gradient. Thermal radiation and conduction heat transfer mechanisms were neglected as a first approximation due to pebble bed characteristics. The effect of the gas pressure was introduced, to our knowledge, for the first time in a DEM code. This represents a step forward for thermal DEM simulations allowing the investigation of the Smoluchowski effect in granular beds. The code was calibrated with existing experimental data obtained in KIT with EU Ref. Parametric studies were carried out to investigate the influence of both skeleton and matrix materials, compressive state of the bed, temperature and pressure of the system. The code was further validated comparing the numerical results with the existing experimental data reported in literature for  $\text{Li}_2\text{TiO}_3$  and  $\text{Li}_2\text{ZrO}_3$  breeder materials.

After the calibration, numerical results perfectly resemble the experimental data reported in literature with all model parameters being physical and measurable quantities. The code predicted the experimental results with a good agreement for different gas type, solid material, temperature, gas pressure and compression state of the bed. No significant influence of the compression state on the effective thermal conductivity was found. The S-shape curve characteristic of the Smoluchowski effect was successfully reproduced. However, the solid material plays a major role in the heat transfer mechanism of a packed bed. In literature, for some of these materials, there are several correlations characterizing the bulk material's thermal conductivity. This results in different values of the effective thermal conductivity predicted by the DEM code. Nevertheless, the authors proved that the code predicted the experimental results carried out on pebbles of  $\text{Li}_2\text{ZrO}_3$ . For this material the correlations reported in various sources lead to the calculation of similar thermal conductivity values in agreement with the experiment.

The influence of the interstitial filling gas type as well as of the gas pressure on the effective thermal conductivity found in the experiments was confirmed. A strong reduction of the effective thermal conductivity of the bed was observed reducing the gas pressure. This means that in case of an accident resulting in a leakage in the breeding zone, the pressure and thus the effective thermal conductivity of the beds is expected to be severely reduced. Therefore, even if a reduction of the purge gas pressure determines a lower permeation of the tritium into the coolant, in turn it decreases the effective thermal conductivity with the consequence increment of the temperatures in the bed. Reducing the gas pressure to very low values, thermal radiation may become a noticeable heat transfer mechanism. However, due to pebble bed characteristics, only a slight increase of the effective thermal conductivity is expected at low pressure compared to the prediction of our current model. Therefore, we are confident that the proposed model is a good approximation of the physical reality especially at BB relevant conditions.

#### References

- [1] A. Ying, et al., Status of ceramic breeder pebble bed thermo-mechanics R&D and impact on breeder material mechanical strength, *Fusion Eng. Des.* 87 (7–8) (2012) 1130–1137.
- [2] Y. Poitevin, et al., Tritium breeder blankets design and technologies in Europe: development status of ITER Test Blanket Modules, test & qualification strategy and roadmap towards DEMO, *Fusion Eng. Des.* 85 (10–12) (2010) 2340–2347.
- [3] G.K. Batchelor, R.W. O'Brien, Thermal or electrical conduction through a granular material, *Proc. R. Soc. Lond. Ser. A* 355 (1682) (1977) 313.
- [4] M. Smoluchowski, Über den Temperatursprung bei Wärmeleitung in Gasen *Pisma Mariana Smoluchowskiego* 1.1, (1924), pp. 113–138.
- [5] M. Enoda, et al., Effective thermal conductivity measurement of the candidate ceramic breeder pebble beds by the hot wire method, *Fusion Technol.* 39 (2001) 612.
- [6] K. Raed, Investigation of Knudsen and Gas-atmosphere Effects on Effective Thermal Conductivity of Porous Media, Ph.D. Thesis, Faculty of Mechanical, Process and Energy Engineering Technische Universität Bergakademie Freiberg, 2013.
- [7] A. Griesinger, et al., Measurements and theoretical modelling of the effective thermal conductivity of zeolites, *Int. J. Heat Mass Transfer* 42 (1999) 4363–4374.
- [8] W. Dai, et al., Influence of gas pressure on the effective thermal conductivity of ceramic breeder pebble beds, *Fusion Eng. Des.* 118 (2017) 45–51.
- [9] Y. Asakuma, et al., Thermal radiation analysis of packed bed by a homogenization method, *Int. J. Heat Mass Transfer* 73 (2014) 97–102.
- [10] Lu, et al., Correlation between structure and thermal conductivity of organic aerogels, *J. Non-Cryst. Solids* 1995 (2016) 226–234.
- [11] H. Wu, et al., Effect of scale on the modeling of radiation heat transfer in packed pebble beds, *Int. J. Heat Mass Transfer* 101 (2016) 562–569.
- [12] S. Papeschi, et al., Effective thermal conductivity of advanced ceramic breeder pebble beds, *Fusion Eng. Des.* 116 (2017) 73–80.
- [13] T.S. Yun, T.M. Evans, Three-dimensional random network model for thermal conductivity in particulate materials, *Comput. Geotech.* 37 (2010) 991–998.
- [14] S. Kanuparthi, et al., An efficient network model for determining the effective thermal conductivity of particulate thermal interface materials, *IEEE Trans. Compon. Packag. Technol.* 31 (September (3)) (2008).
- [15] Y. Gan, M. Kamlah, Discrete element modelling of pebble beds: with application to uniaxial compression tests of ceramic breeder pebble beds, *J. Mech. Phys. Solids* 58 (2010) 129–144.
- [16] R.K. Annabattula, et al., Mechanics of binary and polydispersed spherical pebble assembly, *Fusion Eng. Des.* 87 (2012) 853–858.
- [17] Y. Gan, M. Kamlah, J. Reimann, Computer simulation of packing structure in pebble beds, *Fusion Eng. Des.* 85 (2010) 1782–1787.
- [18] Y. Gan, et al., Thermal discrete element analysis of EU solid breeder blanket subjected to neutron irradiation, *Fusion Sci. Technol.* 66 (2014) p83.
- [19] M.G. Kaganer, *Thermal Insulation in Cryogenic Engineering*, Israel Program for Scientific Translations, Jerusalem, 1969.
- [20] N. Wakao, S. Kagnei, *Heat and Mass Transfer in Packed Beds*, Gordon and Breach, New York, 1982.
- [21] B. Baule, Theoretische behandlung der erscheinungen in verdunnten gasen, *Annalen der Physik* 44 (1914) 145–176.
- [22] F.O. Goodman, thermal accommodation coefficients, *J. Phys. Chem.* 84 (1980) 1431–1445.
- [23] A. Abou-Sena, A. Ying, Effective thermal conductivity of lithium ceramic pebble beds for fusion blankets: a review, *Fusion Technol.* 47 (2005) 1094–1100.
- [24] B. Löbbecke, et al., Thermal conductivity of sintered lithium orthosilicate compacts, *J. Nucl. Mater.* 386–388 (2009) 1068–1070.
- [25] Dr. R. Knitter, Karlsruhe Institute of Technology, personal communication based on the results reported in [20].
- [26] P. Gierszewski, Review of properties of lithium metatitanate, *Fusion Eng. Des.* 39–40 (1998) p.739.
- [27] S. Saito, et al., Density dependence on thermal properties of  $\text{Li}_2\text{TiO}_3$  pellets, *J. Nucl. Mater.* 253 (1998) 213–218.

- [28] P. Gierszewski, Thermal conductivity of lithium metazirconate, *Fusion Technol.* 23 (1993) 333.
- [29] D.A. Moore, A Compilation of Data and a Review of the Properties of Lithium Monoxide and Lithium Zirconates Relevant to Their Use as Tritium Breeder Material in Fusion Reactors, NRL, Springfields, 1989 NRL-R-2014 (S).
- [30] David R. Lide, *CRC Handbook of Chemistry and Physics*, 95th ed., CRC Press, 2004.
- [31] **The Engineering ToolBox**, [http://www.engineeringtoolbox.com/dry-air-properties-d\\_973.html](http://www.engineeringtoolbox.com/dry-air-properties-d_973.html), (18/09/2017).
- [32] S. Papeschi, et al., Numerical and experimental characterization of ceramic pebble beds under cycling mechanical loading, *Fusion Eng. Des.* 112 (2016) 162–116.
- [33] M. Enoda, Y. Ohara, N. Roux, A. Ying, G. Piazza, S. Malang, Effective thermal conductivity measurement of the candidate ceramic breeder pebble beds by the hot wire method, *Fusion Technol.* 39 (612) (2001).
- [34] M. Dalle Donne, A. Goraieb, G. Piazza, G. Sordon, Measurements of the effective thermal conductivity of Li<sub>4</sub>SiO<sub>4</sub> pebble bed, *Fusion Eng. Des.* 49 (2000).
- [35] R. Bauer, E.U. Schlunder, Effective radial thermal conductivity of packings in gas flow. Part II. Thermal conductivity of the packing fraction without gas flow, *Int. Chem. Eng.* 18 (189) (1978).
- [36] R.O.A. Hall, D.G. Martin, The thermal conductivity of powder beds. a model, some measurements on UO<sub>2</sub>, vibro-compacted microspheres, and their correlation, *J. Nucl. Mater.* 101 (1981) 172–183.
- [37] P. Lorenzetto, et al., A European proposal for an ITER water-cooled solid breeder blanket, *Fusion Eng. Des.* 27 (1995) 423–429.
- [38] T. Hatano, et al., Effective thermal conductivity of Al<sub>2</sub>TiO<sub>3</sub> pebble bed for a demo blanket, *Fusion Sci. Technol.* 44 (2003) p94.